



Graphene/ZnO nanocomposite with seamless interface renders photoluminescence quenching and photocatalytic activity enhancement

Huihui Liu¹ , Miaomiao Xiang¹ , and Xiang Shao^{1,2,*}

¹Department of Chemical Physics, University of Science and Technology of China, Hefei 230026, Anhui, China

²CAS Key Laboratory of Urban Pollutant Conversion and Synergetic Innovation Center of Quantum Information and Quantum Physics, University of Science and Technology of China, Hefei 230026, Anhui, China

Received: 22 January 2018

Accepted: 15 June 2018

Published online:
25 June 2018

© Springer Science+Business
Media, LLC, part of Springer
Nature 2018

ABSTRACT

The interface of graphene (G) and oxide can significantly influence the properties and/or applications of the binary system. However, it is usually beyond controllability during the conventional physical intermixing and/or solvothermal preparations. In this article, by directly growing nanocrystalline graphene films on the ZnO nanocrystals through a medium-temperature chemical vapor deposition method utilizing C₂H₂ as the carbon source, we successfully achieved a G/ZnO binary structure with a uniform and contamination-free G/oxide interface. The fabricated G/ZnO powders not only demonstrated a clear charge transfer between graphene and ZnO that leads to photoluminescence quenching, but also manifested an enhanced activity in the photocatalytic degradation of methylene blue when the graphene thickness is optimized. This work has demonstrated the essential significance of the interface control for the functionality of the graphene/semiconductor binary systems.

Introduction

As a promising semiconductor material, ZnO has attracted ever-increasing attention due to its broad applications in field effect transistors [1], light-emitting diodes [2], photoluminescent materials [3], hydrogen production [4], catalysts [5–8], water purification [9–11], sensors [12–14] and so on. Hybridization of carbon materials with ZnO offers a powerful way to realize even more elegant properties

seen in energy storage [15], ultrafast photoelectronics [16], as well as photocatalysis [17, 18]. In particular, graphene (G) has been demonstrated with unique advantages in combining ZnO and achieving significantly enhanced piezoelectricity, photocatalytic activity and electrochemical activity, etc [19–27].

In conventional methods, graphene/ZnO composites (shortened as G/ZnO) are prepared by mixing the graphene oxide (GO) or reduced GO (r-GO) with ZnO particles in solution [18, 27]. In these preparations, it is difficult to achieve uniform contact

Address correspondence to E-mail: shaox@ustc.edu.cn

between graphene and the ZnO substrate. The presence of numerous adsorbates or contaminations (–OH, H₂O, –COOH and so on) [28, 29] between graphene and ZnO cannot be fully avoided, which can severely influence the interface properties and the expandable applications of the G/ZnO composite. Many works have been done in this area with the aim of solving this issue. In 2009, Zheng et al. successfully grew pyramid-like graphene sheets on Ni-coated ZnO nanowires via a “base growth” mechanism using plasma-enhanced chemical vapor deposition (PECVD), with which they obtained a significantly improved field emission (FE) property compared to bare ZnO nanowires [30]. In 2010, Kunook Chung et al. fabricated ZnO nanowall structures on the surface of graphene, providing a platform for studying the physical properties at interfaces between semiconducting nanostructures and graphene [31]. In 2011, Brijesh Kumar et al. reported vertically well-aligned ZnO nanowires and nanowalls can be grown on the graphene substrate under the catalytic effect of the gold catalyst. They claimed that the fabricated piezoelectric nanogenerator can generate a new type of direct current through the specific electron dynamics in the nanowire–nanowall hybrid [32]. Unfortunately, the presence of metal catalyst severely interfered the disclosure of the charge transfer mechanism across the G/ZnO interface. To solve the problem, Ravi K Biroju et al. applied a thermal vapor deposition method to fabricate various one-dimensional (1D) ZnO nanostructures directly on the surfaces of graphene and graphene oxide. By controlling the growth of ZnO in the presence/absence of catalyst, they systematically investigated the photoluminescence properties of the composite [33, 34]. However, due to the specific aspect ratio of the ZnO 1D structure, the contact area between graphene and ZnO was relatively small. In 2017, Hyo-ki Hong et al. developed an atomic layer deposition (ALD) technique and successfully grew a single-atom-thick ZnO layer on graphene, for the first time realized the seamless and uniform interface between graphene and ZnO [35]. Nevertheless, it is an inverted system compared to the more general case of graphene over ZnO. Additionally, the monolayer ZnO may have drastically deviated properties against the bulk material; hence, the composite cannot give out the usual interface property.

Here, we report a novel yet principally simpler method in fabricating the graphene/ZnO composites.

By using C₂H₂ as the precursor for a chemical vapor deposition (CVD), we can directly synthesize graphene adlayers on the surface of ZnO nanocrystals. Because of the applied inert atmosphere as well as the relatively high temperature (around 400 °C), we were able to achieve a uniform cover of graphene on the ZnO surface without intercalated species. Such hybrid structure showed significantly enhanced activity in the photodegradation of methylene blue (MB) as compared to the physical mixture. Photoluminescence measurements indicated that the intimate contact between graphene and ZnO facilitates more efficient electron transfer across the interface (from ZnO to graphene). Moreover, the intimate interface of the binary materials is of great importance for fundamental understanding of the interfacial physical and chemical properties of 2D material and oxide semiconductors.

Experimental

Materials

Zinc acetate dehydrate (Zn(OAc)₂·2H₂O, Sinopharm Chemical Reagent Co., Ltd, AR), sodium hydroxide (NaOH, Aladdin, 96%), deionized water (18.2 MΩ cm), ethanol (CH₃CH₂OH, Sinopharm Chemical Reagent Co., Ltd, 99.7%), graphene oxide (Aladdin, 99%), Ar gas (Linde Industrial Gases, 99.999%), acetylene (Linde Industrial Gases, 99.5%) were all used as-received without further purification.

Preparation of zinc oxide (ZnO) nanoparticles

In a typical procedure, 0.88 g (4 mmol) Zn(OAc)₂·2H₂O was first dissolved in 200 mL ethanol. Then, 4 g (0.1 mol) NaOH was added into the solution and stirred for 2 h to make it completely dissolved at room temperature (RT) [36]. The obtained cloudy solution was sealed and placed in the dark at RT. After 7 days white precipitate was collected by centrifuging the solution at 8000 rpm for 5 min, which was subsequently washed with deionized water and ethanol for several cycles and finally dried at 60 °C in an oven.

Synthesis of graphene/ZnO (G/ZnO) nanocomposites

The CVD syntheses of G/ZnO nanocomposites were performed in a horizontal quartz tube mounted inside a furnace. A typical process is: (1) load the fused silica tube with 100 mg ZnO nanoparticles, heat to 400 °C under an Ar flow of 200 sccm; (2) introduce 1 sccm C₂H₂ and 200 sccm Ar for a period of time; (3) after graphene growth, stop the C₂H₂ gas and anneal for 60 min at 400 °C. Finally, the furnace is cooled to room temperature in Ar flow. The thicknesses of graphene samples can be controlled by varying either the growth time or the loading speed of C₂H₂. The CVD-synthesized samples are denoted as G-*t*/ZnO, wherein *t* is the growth time in minutes. Specifically, G-0/ZnO denotes the blank sample undergoing merely the annealing in Ar yet without C₂H₂ fed in.

Preparation of the mixture of graphene oxide and ZnO (GO-ZnO)

For a comparative study, we also prepared the composites of GO and ZnO (termed as GO-ZnO) by a traditional physical intermixing method. The as-prepared ZnO nanocrystals were firstly annealed at 400 °C in Ar for 120 min. Then, typically 100 mg of the annealed ZnO powder was dispersed in 60 mL deionized water together with a certain amount of GO ranging from 1 to 43 mg, in order to get different mass fractions of GO (1–30%). After sonication for 60 min, the mixtures were centrifuged and dried in a vacuum oven. The dried samples were further annealed at 300 °C in Ar for 2 h.

Photocatalytic activity test

Typically in a performance test, 30 mg photocatalyst (G/ZnO or pure ZnO nanocrystals) was suspended in 100 mL of 3×10^{-5} M methylene blue (MB) solution. The suspension was then sonicated for 5 min and stirred for 1 h in the dark to achieve the adsorption–desorption equilibrium. Under atmospheric environment and stirring, the solution was irradiated using a 200 W Xe lamp (central wavelength of 365 nm). Three mL sample solution was taken after certain intervals during the experiment and centrifuged to remove the catalyst completely. Then, the sample solutions were analyzed on a UV–

Vis spectrophotometer (PERSEE). The percentage of MB degradation is reported as C/C_0 . Here, C is the concentration of unreacted MB solution which is deduced by the intensity of the main absorption peak (~ 664 nm) of each sampling solution, while C_0 is the adsorption of the initial concentration of MB before the UV irradiation is turned on.

Characterization methods

The fabricated graphene adlayers were investigated by a series of characterizations. X-ray photoelectron spectrum (XPS) measurements were performed on an ESCALAB 250 spectrometer (VG Co., UK) with Al K α X-ray radiation as the source for excitation. Transmission electron microscopy (TEM) images were taken by using a JEM-2100F high-resolution transmission electron microscope with an accelerating voltage of 200 kV. All TEM samples were prepared by depositing a drop of diluted suspensions in ethanol on a microgrid copper network. X-Ray diffraction (XRD) patterns of the samples were collected on a TTR-III (Rigaku). Raman spectroscopy was carried out on a LabRam HR Raman spectrometer (Horiba) with 514.5-nm wavelength incident laser source. Photoluminescence spectroscopy measurements were performed on a JY Fluorolog-3-Tou fluorescence spectrometer (Jobin–Yvon, France). The optical properties of the samples were analyzed by ultraviolet–visible diffuse reflectance spectroscopy (UV–Vis DRS) using a SOLID3700 UV–Vis spectrophotometer (Shimadzu Co., Japan). Electron paramagnetic resonance (ESR) spectra were collected on a JES-FA200 (JEOL, Ltd., Japan). The Brunauer–Emmett–Teller (BET) specific surface areas (S_{BET}) were measured by N₂ adsorption at 77 K on a Micromeritics TriStar II apparatus.

Results and discussion

Characterization of the graphene adlayer grown on ZnO nanocrystals

Serving as the substrate, the ZnO nanocrystals with suitable size have been fabricated before subjecting to the CVD growth of graphene. As shown in Fig. S1 and S2, according to the synthetic recipe, both micrometer-sized ZnO rods with well-defined shapes and less-defined small ZnO nanoparticles can be

synthesized with narrow distribution in size. The micrometer-sized ZnO (see supporting information for its synthesis recipe) has obvious advantages in thermal stability and can persist the well-defined shape during the CVD process. However, they also inevitably suffer the difficulties in characterizing the structures of the surface. Therefore, we prefer to use the small nanocrystals with relatively irregular shapes as the substrate for graphene growth which can be imaged readily under the TEM. In the following, we will mainly focus on the nanocrystal samples with sizes of 20–40 nm.

Figure 1a–c shows the high-resolution TEM images of the ZnO nanoparticles after subjected to the CVD processes. As indicated by the yellow arrows, we can clearly identify the formation of the graphene adlayers whose thickness evolves as a function of growth time (GT). In particular, when GT is shorter than 30 min, the ZnO nanocrystals present no recognizable adspecies on the surfaces, as shown in Fig. 1a. When GT reaches 60 min, as shown in Fig. 1b, already one or two graphene adlayers can be observed under the TEM imaging. Extending the GT until 120 min (Fig. 1c) leads to the formation of thicker graphene film around 2–3 layers in average. (More TEM evidences can be found in Figs. S3 and S4 in the supporting information.) Thus, the growth speed can be roughly estimated as 1 monolayer per hour. Importantly, under all circumstances we found the graphene films uniformly wrapping the ZnO surface. Especially, the first layer contact with the ZnO surface without any observable gap, manifesting a seamless interface between graphene and ZnO nanocrystals.

In addition to the developed graphene adlayers, the TEM images also present the lattice of the ZnO nanocrystals, wherein the (002) planes of the wurtzite ZnO crystal can be clearly identified, dictating the

intact crystalline phase of ZnO after CVD synthesis. To confirm that, we have conducted XRD measurements to check the crystallinity of the ZnO powder after CVD treatments. Figure 2 shows the XRD patterns collected on a series of ZnO samples varied with CVD time. One can find that before and after CVD growth the XRD diffractions of the ZnO nanoparticles are almost identical at the diffraction positions. The XRD pattern for the synthesized ZnO perfectly matches with the JCPDS data for a wurtzite structure. All the peaks, positioning at 31.8, 34.4, 36.3, 47.5, 56.6, 62.9 and 68.0 degrees, can find perfect correspondences to the crystal planes of (100), (002), (101), (102), (110), (103) and (112) of a wurtzite ZnO, respectively [37]. One may notice that the intensities of the XRD diffractions get gradually weakened along with the extension of the growth time. This may be due to the partial screening of the diffraction signals by the accumulated graphene adlayers. In addition, we found the shape of the ZnO nanocrystals has actually changed during the CVD process, as shown in Fig. S5, possibly due to the sintering effect under elevated temperature. In contrast to the well-resolved ZnO diffractions, we did not see any obvious diffraction peaks coming from graphene adlayers ($\sim 2\theta = 25.6^\circ$ marked as # in Fig. 2) [38]. This is because the graphene adlayer is too thin to give detectable signals, as revealed by the TEM images.

Raman spectroscopy is sensitive to the crystallization as well as structural disorders and defects in nanostructures, and has been widely applied in characterizing various carbonaceous nanostructures in particular graphene [39]. Therefore, we have performed Raman spectroscopy studies to reveal the structural details of the as-fabricated G/ZnO nanocomposite. Figure S6 shows the Raman spectrum for the blank ZnO, from which we can confirm the wurtzite structure of the synthesized ZnO. The

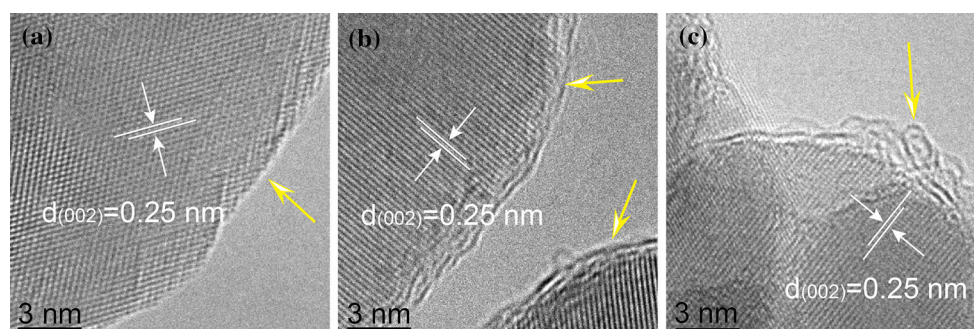


Figure 1 High-resolution TEM images of G/ZnO composites prepared by different growth time. **a** 30 min; **b** 60 min and **c** 120 min.

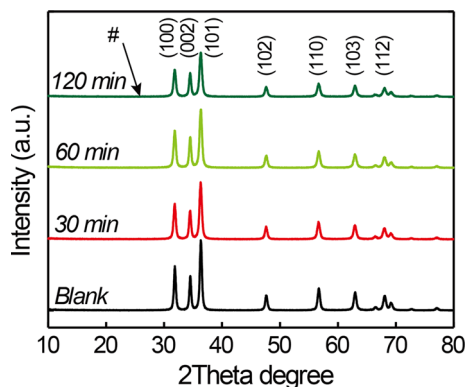


Figure 2 X-ray diffraction (XRD) pattern of G/ZnO composites prepared by different growth time: 30, 60 and 120 min, respectively.

Raman spectra of the G/ZnO composites obtained with 60 min and 120 min CVD growth (termed as G-60/ZnO and G-120/ZnO, respectively) are shown in Fig. 3, which present an increased evolution of the two main bands at both 1370 and 1600 cm^{-1} in comparison with blank ZnO nanocrystals. These two bands perfectly fit the positions of the representing D and G bands of an r-GO or nanocrystalline graphene [40, 41]. The D band at around 1370 cm^{-1} is well known in the carbon materials and corresponds to structural defects [42]. The G band at around 1600 cm^{-1} is correlated with the scattering of the E_{1g} phonon of the sp^2 carbon atoms hence characteristic of the sp^2 - sp^2 bonds [43]. On the G-30/ZnO sample that was prepared by 30 min CVD growth, however, we did not observe any D- or G-band features in the corresponding Raman spectrum, indicating that probably no sizable carbon structures have been formed within such short time, as also revealed by

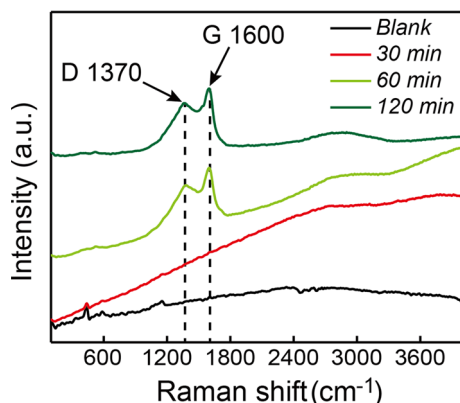


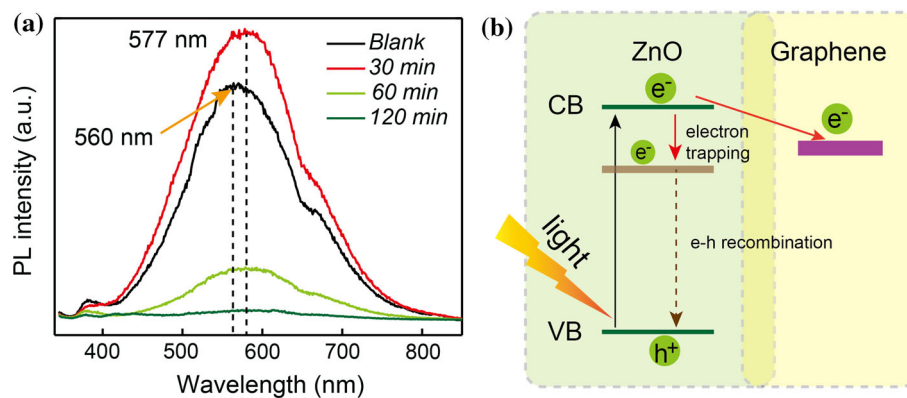
Figure 3 The Raman spectra for ZnO and G/ZnO nanocomposites with different growth time.

the TEM image shown in Fig. 1. The Raman spectra can be further subjected to detailed deconvolution analysis to derive more quantitative information, as can be found in Fig. S7 and Table S1. The full-width half-maximum (FWHM) of the deconvoluted G band has reciprocal relationship with the in-plane crystallinity. The lower the FWHM, the higher the degree of crystallization [44]. Consequently, the crystallization of the graphene adlayer in G-120/ZnO should be much better than in G-60/ZnO since the former has smaller FWHM for the G band. The domain size can also be estimated by $L_a = (2.4 \times 10^{-10}) \lambda^4 / (I_D/I_G)^{-1}$ [45], wherein L_a is the averaged diameter of the graphene domains, λ the wavelength of the applied laser, I_D and I_G the intensity of the deconvoluted D band and G band, respectively. As can be found in Table S1, the calculated grain size of G-60/ZnO is about 5.3 nm, while for G-120/ZnO about 7.4 nm. These values should only be taken as rough estimations. But they correctly reflect the fact that the fabricated graphene adlayers over the ZnO nanoparticles have a nanocrystalline nature. In a control experiment, we have synthesized graphene films on the ZnO(0001) single-crystal surfaces by following exactly the same recipe (i.e., the same CVD apparatus, the same flow rate and gas ratio, the same growth temperature, etc.) as for growing graphene on the ZnO nanoparticles. Figure S8 shows the characterization results of the particular sample grown for 120 min, wherein the nanocrystallinity of the graphene film can be unambiguously confirmed and the domain sizes were found in good consistency with the Raman estimations.

Tailored properties of the G/ZnO composite

After proving the fabrication of the G/ZnO nanocomposite, it would be of more importance to examine the characteristic properties of a seamless G/ZnO interface. Using the 325-nm laser beam as the excitation light, we were able to collect a series of photoluminescence spectra of the G/ZnO samples. As shown in Fig. 4a, for blank ZnO nanocrystals a broad yellow-green band ranging from 450 to 800 nm and peaking at $\sim 577\text{ nm}$ is detected, which is usually attributed to the emissions mediated by oxygen vacancies in the ZnO lattice [46]. This proposition is supported by our control experiments as shown in Fig. S9. We treated the bare ZnO nanocrystals under same CVD conditions but without acetylene in

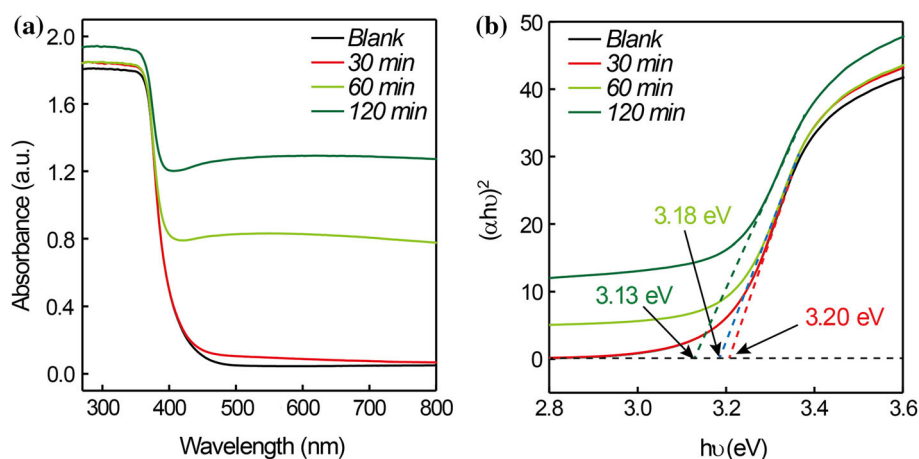
Figure 4 **a** Room temperature photoluminescence for ZnO and G/ZnO nanocomposites with different growth time. **b** Schematic illustrating the mechanism of charge separation over the G/ZnO nanocomposites.



presence, and found this luminescence band increased along with the CVD time, clearly indicating a defect-mediated nature. For the G-30/ZnO sample, an increased emission was observed, which can be attributed to the increased recombination centers other than any graphitic species that were formed on the ZnO surface according to both TEM and Raman results. In contrast, when sufficiently sizable graphene structures have been established on the ZnO surface, such as the G-60/ZnO and G-120/ZnO samples, the intensity of the luminescence bands significantly decreased until fully quenched in the range of 450–800 nm. Therefore, such changes of luminescence intensity clearly reflect that the presence of graphene efficiently suppresses the defect-mediated electron–hole recombination events within the ZnO material. Such effect should originate from the superior electron conductivity of graphene as well as its comparable work function as the oxide semiconductors. As schemed in Fig. 4b, here graphene is proposed to serve as an electron sink and assist the separation of the photoexcited charge carriers by quickly shuttling away the electrons across the interface. For the bare ZnO and the sample without sizable graphene attached such as G-30/ZnO, the photoexcited electrons are predominantly trapped by the defect states, which then decay by recombining with the holes accompanied by luminescence. After certain amount of graphene has been formed on ZnO surface, a new electron transfer channel is opened, which quickly transfers away the photo-induced electrons. As a result, the defect-mediated luminescence also gets weakened. In this scenario, the thicker the graphene, the more significant the effect. This effect would finally benefit the photocatalytic activity of the G/ZnO nanocomposites, as will be shown below.

The attachment of graphene adlayer on the ZnO surface not only changes the latter's light-emitting property, but should also tailor its absorptive properties to the incident light, which can significantly broaden the photocatalytic applications of the ZnO materials. Figure 5a shows the UV–Vis spectra that have been collected on a series of G/ZnO samples. One can immediately recognize that the presence of graphene greatly increases the absorbance in the visible light region ranging from 400 to 800 nm. And this increment positively correlates with the growth time in term of graphene thickness. The plot can be further transformed via the Kubelka–Munk function [47] into the form as shown in Fig. 5b. By extending the tangent at the inflection point of each curve to the abscissa, the optical band gap of the composite material can be estimated. As shown in Fig. 5b, the band gap of the pristine ZnO is measured as 3.20 eV, coincides with what generally reported for ZnO. With the growth of graphene on the surface, the band gap of the composite has been gradually reduced to 3.18 eV for G-60/ZnO and 3.13 eV for G-120/ZnO. As mentioned before, in a series of control experiments the ZnO nanocrystals were performed with CVD treatments in the absence of acetylene. Although the luminescence spectra (Fig. S9) indicated an apparent bulk reduction; however, no obvious changes of the ZnO band gap have been observed (Fig. S10). Therefore, such slight band gap narrowing can be reasonably attributed to the chemical interactions between graphene and the ZnO surface [38, 48], particularly through the chemical bonding formed at the defects or domain boundaries of the synthesized graphene which in turn cause the charge redistribution at the interface locally and meantime the band gap reduction of ZnO.

Figure 5 **a** UV–Vis spectra on the blank ZnO and with CVD-synthesized graphene for different growth times. **b** Kubelka–Munk estimation of the band gaps of blank ZnO and G/ZnO.



The electronic influence of graphene over the ZnO substrate may also induce the changes of the core levels of surface atoms, thus can be detected by X-ray photoelectron spectroscopy. A typical survey spectrum of the G-60/ZnO sample is shown in Fig. S11a, wherein no clues of any additional metallic species (e.g., Ni, Cu and Pt) can be observed on the sample, indicating that the entire process is free of metal catalyst. In Figs. S11b and S11c, we present a detailed analysis of both the C1s and O1s XPS spectra of the G-60/ZnO sample. One can clearly see that the C1s spectrum consists of a sharp peak at 284.7 eV that corresponds to C–C/C=C bond and two weak peaks at 286.6, 288.9 eV which are normally assigned to C–O and C=O species, respectively [49, 50]. These specific transitions dictate the nanocrystalline nature of our fabricated graphene whose defects or domain boundaries can be readily reacted after exposing to ambient. The O1s spectrum was deconvoluted into three peaks at 530.3, 531.5 and 532.5 eV, corresponding to the O^{2-} ions in the wurtzite structure (Zn–O) [51], oxygen vacancy (V_o) [52] and chemisorbed oxygen on the surface [53], respectively. Figure 6a–c shows the high-resolution C1s, O1s and Zn 2p XPS spectra of a series of G/ZnO samples, respectively. Notice that the main peak of C1s has been arbitrarily fixed to 284.7 eV and used as a reference; therefore, it is not possible to differentiate from the carbon impurities produced during air exposure [54]. Under this condition, the shifts of the O1s and Zn 2p core levels can still be correlated with the increasing attachments of the graphene adlayers. The G-30/ZnO sample shows almost identical XPS signals as the blank ZnO nanocrystals in that no recognizable graphene structures have been formed.

When sizable graphene adlayers were developed, as for the G-60/ZnO and G-120/ZnO samples, significant blue shifts were observed for both O1s and Zn 2p. More specifically, the two characteristic core levels synchronically shift by 0.4–0.5 eV for G-60/ZnO sample and 0.8–0.9 eV for G-120/ZnO sample, respectively, while the shapes of the emission peaks remain unchanged (see Fig. S12). Such concomitant blue shifts of both anion and cations indicate a strong field effect established at the interface of graphene and ZnO that points to the inside of ZnO substrate. Previously we reported similar phenomenon for the graphene adlayers synthesized over the atomically flat rutile-TiO₂ single crystals through similar CVD process [55]. In consideration of the relatively lower work function of graphene than the ZnO material (4.5 vs. \sim 4.7 eV) [56, 57], the former has large tendency to donate electrons to the latter when they come in contact. The produced net charges at the two sides of the interface build up a dipole field which hence forces the downshifts of the energy levels of both O and Zn ions. Consequently, the binding energies of both O1s and Zn 2p are raised. And the tendency increases along with more graphene attached.

By carefully examining the sequence of the high-resolution Zn 2p and O1s XPS spectra, we did not see any reduced species even though the synthetic condition is highly reductive. This can be due to the sublimation of Zn at the CVD temperature (hence no net oxygen vacancies can be formed), but can also be due to the relatively low concentration of these species. Considering the paramagnetic nature of these species, we resorted to more sensitive technique such as EPR to characterize the structural changes of the ZnO nanocrystals upon CVD process. Figure 7a

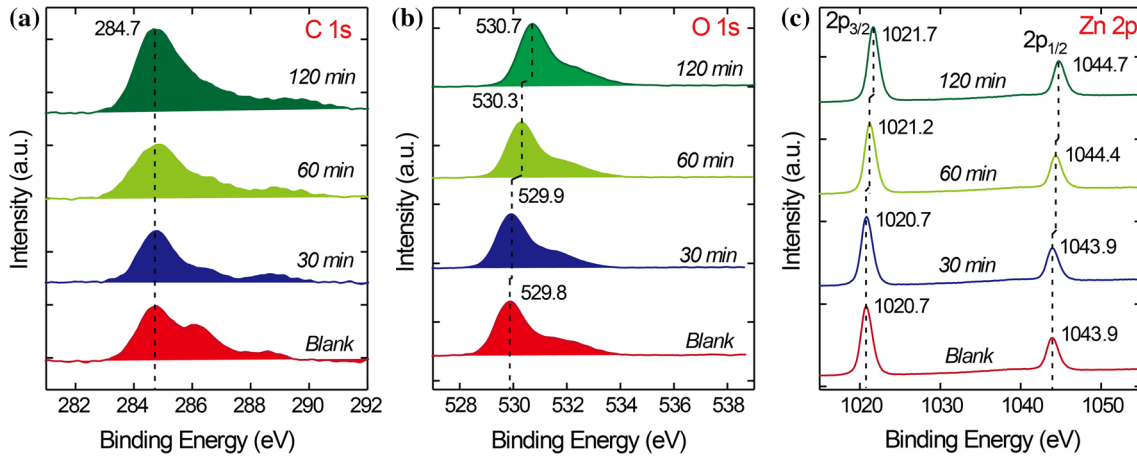
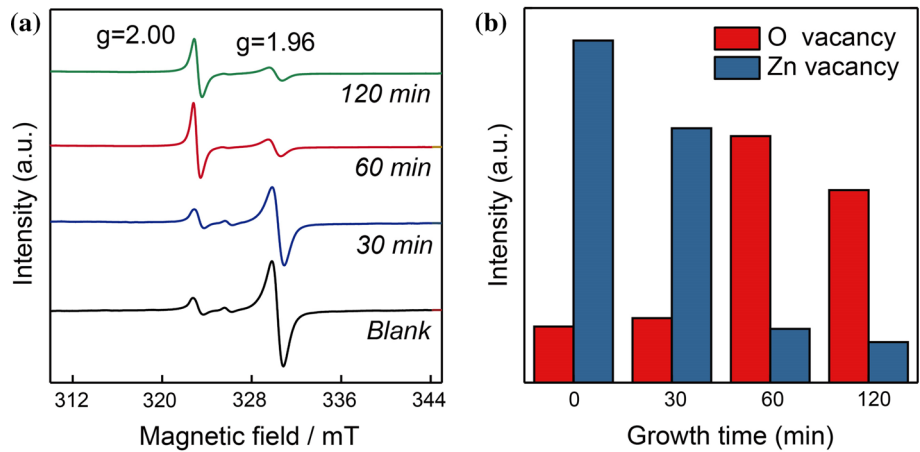


Figure 6 XPS spectra of the CVD-synthesized G/ZnO composites. **a** C1s; **b** O1s and **c** Zn 2p evolutions against the CVD growth time.

Figure 7 a EPR spectra for ZnO and G/ZnO nanocomposites with different growth time. **b** The trend of oxygen vacancy and zinc vacancy with the growth time.



shows the EPR spectra collected on the same series of samples as characterized with the above techniques. Two main resonance signals can be identified at $g = 2.00$ and $g = 1.96$, respectively. Their peak-to-peak heights were directly used to evaluate the concentration of the spin centers [58, 59]. The resonance of $g = 1.96$ is usually attributed to Zn vacancies (V_{zn}^-) inside the ZnO nanocrystals [60, 61]. It dominates in the blank sample and quickly decreases at the beginning of the CVD growth of graphene. When sufficiently thick graphene adlayers have been formed, the signal intensity, i.e., the concentration of V_{zn}^- remains roughly constant, as can be found by comparing the G-60/ZnO and G-120/ZnO samples. In contrast, the resonance around $g = 2.00$ is usually correlated with the oxygen vacancies (V_o) [62, 63]. It shows weak intensity for both the blank and G-30/ZnO samples, but quickly increase until full monolayer of graphene has been formed, such as on the G-60/ZnO. Therefore, the evolution of both $g = 1.96$

and $g = 2.00$ resonances with the CVD growth time actually reflects the evolution of V_{zn}^- and V_o species in the G/ZnO nanocomposites, as plotted in Fig. 7b. Notice that the blank sample is not the as-synthesized ZnO crystals, but those have undergone the similar CVD procedure but without C_2H_2 in presence. Considering the operating temperature around $400\text{ }^\circ\text{C}$, the Zn atoms/ions may readily desorb during the CVD thus lead to the formation of significant amount of V_{zn}^- . When C_2H_2 was induced into the CVD operation, i.e., for the real graphene growth procedure, oxygen atom/ions start to be removed from both the ZnO surface and ZnO bulk. Concomitantly, V_{zn}^- is transformed into $(Zn-O)_v$ and then dismissed due to the annealing effect. Along with the going of the reaction, more oxygen atoms are removed and the V_o species start to grow and saturate until the formation of full monolayer of graphene. From this point, further reactions only lead to the accumulation of more graphene adlayers on the surface yet no loss of

oxygen atoms anymore from the ZnO. On the other hand, the annealing effect continues to work and cause the healing of the various vacancies including the V_o . Therefore, we observed a slightly reduced signal of V_o on the G-120/ZnO sample. It needs to be pointed out that although the formation of V_o is not preferred for bare ZnO, but may become a thermodynamically stable species in the G/ZnO composites under the stabilization of graphene.

Photocatalytic activity of the fabricated G/ZnO nanocomposites

As confirmed by a variety of characterizations, the uniform and seamless contact between graphene adlayer and the ZnO nanocrystal obviously improves the charge transfer between the two materials. It also significantly enhances the absorbability of visible light. One would naturally expect to see an enhanced photocatalytic activity for proper reactions such as photodegradation of methylene blue (MB). As shown in Fig. 8, MB alone shows very slow self-degradation under UV irradiation. In contrast, a significant speedup can be seen after ZnO catalysts were added into the solution. In addition, the G-60/ZnO and G-120/ZnO nanocomposites present a superior activity in the photodegradation of MB solution than blank ZnO nanocrystals. Whereas the G-30/ZnO sample gave reduced activity than the blank sample there have been no sizable graphene structures formed on this sample. We also notice that the G-120/ZnO sample gave slightly reduced activity as compared with G-60/ZnO, indicating the existence of an optimistic thickness of the graphene adlayer. Such self-limited effects generally exist in many systems and are mostly related to a number of competing factors in determining the reaction rates. Here in the photodegradation of MB solution, density of

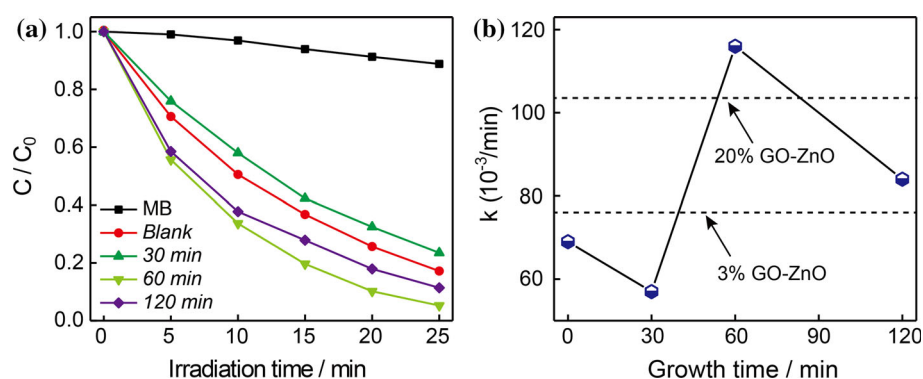
electron/holes, the availability of reaction sites, as well as the absorbability of the reactants, etc., all together lead to the observed phenomenon that one to two layers of graphene on ZnO gave the best activity. Despite the unrevealed reaction mechanism, the net promotion effect of graphene over the ZnO nanocrystals can be undoubtedly verified.

As a comparison with the currently synthesized G/ZnO composites, we also examined the catalytic activities of a series of physical mixtures of graphene oxide (GO) and ZnO (termed as GO-ZnO, see Fig. S13). As shown in Fig. 8b, with the same amount of catalyst, the optimized GO-ZnO mixture with a GO fraction of 20% turned out to degrade MB with less efficiency compared with the G-60/ZnO nanocomposite. On the other hand, we estimated the ratio of graphene to ZnO in our G-60/ZnO sample as about 3% based on the measured surface area ($S_{\text{BET}} \sim 22 \text{ m}^2/\text{g}$) and postulating the averaged thickness of graphene as monolayer (according to the TEM image in Fig. 1b). Notice that this estimation is very rough since neither the graphene adlayers are completely even nor the ZnO nanocrystals are in perfect shape and size. Nevertheless, based on this postulation, one can find in Fig. 8b that the 3% mixture of GO-ZnO gave remarkably lower reaction rate coefficient than the G-60/ZnO sample. In all, these results demonstrate that the seamless contact of graphene and ZnO can indeed provide the optimal configuration for achieving the best photocatalytic activities.

Conclusion

In conclusion, we have successfully developed a metal-free CVD method to fabricate a uniformly coated graphene/ZnO nanocomposite. By using

Figure 8 **a** Liquid-phase photocatalytic degradation of methylene blue (MB) under the irradiation of UV light for blank ZnO and G/ZnO nanocomposites with different growth time. **b** Plot of the reaction rate coefficient k versus the growth time.



C₂H₂ as the precursor and at moderate growth temperature of around 400 °C, we are able to achieve a seamless and contamination-free graphene/ZnO interface. Both photoluminescence spectra and XPS measurements confirm that the optimized graphene/ZnO contact effectively improves the efficiency of charge transfer between the two materials. These properties greatly benefit the photocatalytic activity of the combined system which gets confirmed by the photodegradation of MB molecules in water solution. This work has demonstrated that the interface control can be important in understanding other practical binary systems consisting of two-dimensional materials and semiconductors.

Acknowledgements

We are grateful for the financial support of the NSFC (91545128, 21333001), the MOST (2014CB932700) and the Thousand Talent Program for Young Outstanding Scientists of the Chinese government.

Compliance with ethical standards

Conflicts of interest There are no conflicts to declare.

Electronic supplementary material: The online version of this article (<https://doi.org/10.1007/s10853-018-2605-9>) contains supplementary material, which is available to authorized users.

References

- [1] Arnold MS, Avouris P, Pan ZW, Wang ZL (2003) Field-effect transistors based on single semiconducting oxide nanobelts. *J Phys Chem B* 107:659–663
- [2] Tsukazaki A, Ohtomo A, Onuma T, Ohtani M, Makino T, Sumiya M, Ohtani K, Chichibu SF, Fuke S, Segawa Y, Ohno H, Koinuma H, Kawasaki M (2005) Repeated temperature modulation epitaxy for p-type doping and light-emitting diode based on ZnO. *Nat Mater* 4:42–46
- [3] Koida T, Chichibu SF, Uedono A (2003) Correlation between the photoluminescence lifetime and defect density in bulk and epitaxial ZnO. *Appl Phys Lett* 82:532–534
- [4] Kargar A, Jing Y, Kim SJ, Riley CT, Pan X, Wang D (2013) ZnO/CuO heterojunction branched nanowires for photoelectrochemical hydrogen generation. *ACS Nano* 7:11112–11120
- [5] Fujitani T, Nakamura J (1998) The effect of ZnO in methanol synthesis catalysts on Cu dispersion and the specific activity. *Catal Lett* 56:119–124
- [6] Ong CB, Ng LY, Mohammad AW (2018) A review of ZnO nanoparticles as solar photocatalysts: synthesis, mechanisms and applications. *Renew Sust Energ Rev* 81:536–551
- [7] Zhai BG, Huang YM (2016) A review on recent progress in ZnO based photocatalysts. *Optoelectron Mater* 1:22–36
- [8] Qi K, Cheng B, Yu J, Ho W (2017) Review on the improvement of the photocatalytic and antibacterial activities of ZnO. *J Alloys Compd* 727:792–820
- [9] Li B, Cao H (2011) ZnO@graphene composite with enhanced performance for the removal of dye from water. *J Mater Chem* 21:3346–3349
- [10] Panthi G, Park M, Kim HY, Lee SY, Park SJ (2015) Electrospun ZnO hybrid nanofibers for photodegradation of wastewater containing organic dyes: a review. *J Ind Eng Chem* 21:26–35
- [11] Fu D, Han G, Chang Y, Dong J (2012) The synthesis and properties of ZnO–graphene nano hybrid for photodegradation of organic pollutant in water. *Mater Chem Phys* 132:673–681
- [12] Luo X, Lou Z, Wang L, Zheng X, Zhang T (2014) Fabrication of flower-like ZnO nanosheet and nanorod-assembled hierarchical structures and their enhanced performance in gas sensors. *N J Chem* 38:84–89
- [13] Kim HW, Kwon YJ, Mirzaei A, Kang SY, Choi MS, Bang JH, Kim SS (2017) Synthesis of zinc oxide semiconductors-graphene nanocomposites by microwave irradiation for application to gas sensors. *Sens Actuat B* 249:590–601
- [14] Zhu L, Zeng W (2017) Room-temperature gas sensing of ZnO-based gas sensor: a review. *Sens Actuat A* 267:242–261
- [15] Zhu J, Yang D, Yin Z, Yan Q, Zhang H (2014) Graphene and graphene-based materials for energy storage applications. *Small* 10:3480–3498
- [16] Soci C, Zhang A, Xiang B, Dayeh SA, Aplin DPR, Park J, Bao XY, Lo YH, Wang D (2007) ZnO nanowire UV photodetectors with high internal gain. *Nano Lett* 7:1003–1009
- [17] Han C, Yang MQ, Weng B, Xu YJ (2014) Improving the photocatalytic activity and anti-photocorrosion of semiconductor ZnO by coupling with versatile carbon. *Phys Chem Chem Phys* 16:16891–16903
- [18] Chen D, Wang D, Ge Q, Ping G, Fan M, Qin L, Bai L, Lv C, Shu K (2015) Graphene-wrapped ZnO nanospheres as a photocatalyst for high performance photocatalysis. *Thin Solid Films* 574:1–9

- [19] Shin DM, Tsege EL, Kang SH, Seung W, Kim SW, Kim HK, Hong SW, Hwang YH (2015) Freestanding ZnO nanorod/graphene/ZnO nanorod epitaxial double heterostructure for improved piezoelectric nanogenerators. *Nano Energy* 12:268–277
- [20] Cai R, Wu J, Sun L, Liu Y, Fang T, Zhou S, Li S, Wang Y, Guo L, Zhao C, Wei A (2016) 3D graphene/ZnO composite with enhanced photocatalytic activity. *Mater Des* 90:839–844
- [21] Wei A, Xiong L, Sun L, Liu Y, Li W, Lai W, Liu X, Wang L, Huang W, Dong X (2013) One-step electrochemical synthesis of a graphene–ZnO hybrid for improved photocatalytic activity. *Mater Res Bull* 48:2855–2860
- [22] Herring NP, Almahoudi SH, Olson CR, El-Shall MS (2012) Enhanced photocatalytic activity of ZnO–graphene nanocomposites prepared by microwave synthesis. *J Nanopart Res* 14:1277
- [23] Luo QP, Yu XY, Lei BX, Chen HY, Kuang DB, Su CY (2012) Reduced graphene oxide-hierarchical ZnO hollow sphere composites with enhanced photocurrent and photocatalytic activity. *J Phys Chem C* 16:8111–8117
- [24] Chen TT, Chang IC, Yang MH, Chiu HT, Lee CY (2013) The exceptional photo-catalytic activity of ZnO/RGO composite via metal and oxygen vacancies. *Appl Catal B Environ* 142:442–449
- [25] Wu X, Wen L, Lv K, Deng K, Tang D, Ye H, Du D, Liu S, Li M (2015) Fabrication of ZnO/graphene flake-like photocatalyst with enhanced photoreactivity. *Appl Surf Sci* 358:130–136
- [26] Rokhsat E, Akhavan O (2016) Improving the photocatalytic activity of graphene oxide/ZnO nanorod films by UV irradiation. *Appl Surf Sci* 371:590–595
- [27] Bai X, Sun C, Liu D, Luo X, Li D, Wang J, Wang N, Chang X, Zong R, Zhu Y (2017) Photocatalytic degradation of deoxynivalenol using graphene/ZnO hybrids in aqueous suspension. *Appl Catal B Environ* 204:11–20
- [28] Marlinda AR, Huang NM, Muhamad MR, An'amt MN, Chang BYS, Yusoff N, Harrison I, Lim HN, Chia CH, Vijay Kumar S (2012) Highly efficient preparation of ZnO nanorods decorated reduced graphene oxide nanocomposites. *Mater Lett* 80:9–12
- [29] Park KW, Jung JH (2012) Spectroscopic and electrochemical characteristics of a carboxylated graphene–ZnO composites. *J Power Sour* 199:379–385
- [30] Zheng WT, Ho YM, Tian HW, Wen M, Qi JL, Li YA (2010) Field emission from a composite of graphene sheets and ZnO nanowires. *J Phys Chem C* 113:9164–9168
- [31] Chung K, Lee CH, Yi GC (2010) Transferable GaN layers grown on ZnO-coated graphene layers for optoelectronic devices. *Science* 330:655–657
- [32] Kumar B, Lee KY, Park HK, Chae SJ, Lee YH, Kim SW (2011) Controlled growth of semiconducting nanowire, nanowall, and hybrid nanostructures on graphene for piezoelectric nanogenerators. *ACS Nano* 5:4197–4204
- [33] Biroju RK, Giri PK, Dhara S, Imakita K, Fujii M (2013) Graphene-assisted controlled growth of highly aligned ZnO nanorods and nanoribbons: growth mechanism and photoluminescence properties. *ACS Appl Mater Int* 6:377–387
- [34] Biroju RK, Tilak N, Rajender G, Dhara S, Giri PK (2015) Catalyst free growth of ZnO nanowires on graphene and graphene oxide and its enhanced photoluminescence and photoresponse. *Nanotechnology* 26:145601
- [35] Hong HK, Jo J, Hwang D, Lee J, Kim NY, Son S, Kim JH, Jin MJ, Jun YC, Ermi R, Kwak SK, Yoo JW, Lee Z (2017) Atomic scale study on growth and heteroepitaxy of ZnO monolayer on graphene. *Nano Lett* 17:120–127
- [36] Cao HL, Qian XF, Gong Q, Du WM, Ma XD, Zhu ZK (2006) Shape-and size-controlled synthesis of nanometre ZnO from a simple solution route at room temperature. *Nanotechnology* 17:3632–3636
- [37] Thein MT, Pung SY, Aziz A, Itoh M (2015) Stacked ZnO nanorods synthesized by solution precipitation method and their photocatalytic activity study. *J Sol-Gel Sci Technol* 74:260–271
- [38] Chen Z, Zhang N, Xu YJ (2013) Synthesis of graphene–ZnO nanorod nanocomposites with improved photoactivity and anti-photocorrosion. *CrystEngComm* 15:3022–3030
- [39] Ferrari AC (2007) Raman spectroscopy of graphene and graphite: disorder, electron–phonon coupling, doping and nonadiabatic effects. *Solide State Commun* 143:47–57
- [40] Ramesha GK, Sampath S (2009) Electrochemical reduction of oriented graphene oxide films: an in situ Raman spectroelectrochemical study. *J Phys Chem C* 113:7985–7989
- [41] Liu H, Chen Z, Zhang L, Zhu D, Zhang Q, Luo Y, Shao X (2018) Graphene grown on anatase-TiO₂ nanosheets: enhanced photocatalytic activity on basis of a well-controlled interface. *J Phys Chem C* 122:6388–6396
- [42] Wang J, Chen Z, Chen B (2014) Adsorption of polycyclic aromatic hydrocarbons by graphene and graphene oxide nanosheets. *Environ Sci Technol* 48:4817–4825
- [43] Zhou Y, Bao Q, Tang LAL, Zhong Y, Loh KP (2009) Hydrothermal dehydration for the “green” reduction of exfoliated graphene oxide to graphene and demonstration of tunable optical limiting properties. *Chem Mater* 21:2950–2956
- [44] Jawhari T, Roid A, Casado J (1995) Raman spectroscopic characterization of some commercially available carbon black materials. *Carbon* 33:1561–1565
- [45] Cancado LG, Takai K, Enoki T, Endo M, Kim YA, Mizusaki H, Jorio A, Coelho LN, Magalhães-Paniago R, Pimenta MA

- (2006) General equation for the determination of the crystallite size L_a of nanographite by Raman spectroscopy. *Appl Phys Lett* 88:163106
- [46] Williams G, Kamat PV (2009) Graphene – semiconductor nanocomposites: excited-state interactions between ZnO nanoparticles and graphene oxide. *Langmuir* 25:13869–13873
- [47] Kubelka P, Munk F (1931) An article on optics of paint layers. *Z Tech Phys* 12:593–601
- [48] Ahmad M, Ahmed E, Hong ZL, Xu JF, Khalid NR, Elhissi A, Ahmed W (2013) A facile one-step approach to synthesizing ZnO/graphene composites for enhanced degradation of methylene blue under visible light. *Appl Surf Sci* 274:273–281
- [49] Liu S, Wang Z, Zhang Y, Dong Z, Zhang T (2015) Preparation of zinc oxide nanoparticle–reduced graphene oxide–gold nanoparticle hybrids for detection of NO_2 . *RSC Adv* 5:91760–91765
- [50] Jin JE, Lee JH, Choi JH, Jang HK, Na J, Whang D, Kim DH, Kim GT (2016) Catalytic etching of monolayer graphene at low temperature via carbon oxidation. *Phys Chem Chem Phys* 18:101–109
- [51] Deng D, Martin ST, Ramanathan S (2010) Synthesis and characterization of one-dimensional flat ZnO nanotower arrays as high-efficiency adsorbents for the photocatalytic remediation of water pollutants. *Nanoscale* 2:2685–2691
- [52] Park SM, Ikegami T, Ebihara K (2006) Effects of substrate temperature on the properties of Ga-doped ZnO by pulsed laser deposition. *Thin Solid Films* 513:90–94
- [53] Zhang J, Gao D, Yang G, Zhang J, Shi Z, Zhang Z, Zhu Z, Xue D (2011) Synthesis and magnetic properties of Zr doped ZnO nanoparticles. *Nanoscale Res Lett* 6:587
- [54] Xue Y, Wu B, Jiang L, Guo Y, Huang L, Chen J, Tan J, Geng D, Luo B, Hu W, Yu G, Liu Y (2012) Low temperature growth of highly nitrogen-doped single crystal graphene arrays by chemical vapor deposition. *J Am Chem Soc* 134:11060–11063
- [55] Liu H, Zhu D, Shi H, Shao X (2016) Fabrication of a contamination-free interface between graphene and TiO_2 single crystals. *ACS Omega* 1:168–176
- [56] Giovannetti G, Khomyakov PA, Brocks G, Karpan VM, Van den Brink J, Kelly PJ (2008) Doping graphene with metal contacts. *Phys Rev Lett* 101:026803
- [57] Allen MW, Swartz CH, Myers TH, Veal TD, McConville CF, Durbin SM (2010) Bulk transport measurements in ZnO: the effect of surface electron layers. *Phys Rev B* 81:075211
- [58] Repp S, Erdem E (2016) Controlling the exciton energy of zinc oxide (ZnO) quantum dots by changing the confinement conditions. *Spectrochim Acta A* 152:637–644
- [59] Schneider JJ, Hoffmann RC, Engstler J, Dilfer S, Klyszcz A, Erdem E, Jakes P, Eichel RA (2009) Zinc oxide derived from single source precursor chemistry under chimie douce conditions: formation pathway, defect chemistry and possible applications in thin film printing. *J Mater Chem* 19:1449–1457
- [60] Pham CV, Repp S, Thomann R, Krueger M, Weber S, Erdem E (2016) Charge transfer and surface defect healing within ZnO nanoparticle decorated graphene hybrid materials. *Nanoscale* 8:9682–9687
- [61] Kaftelen H, Ocakoglu K, Thomann R, Tu S, Weber S, Erdem E (2012) EPR and photoluminescence spectroscopy studies on the defect structure of ZnO nanocrystals. *Phys Rev B* 86:014113
- [62] Drouilly C, Krafft JM, Averseng F, Casale S, Bazer-Bachi D, Chizallet C, Lecocq V, Vezin H, Lauron-Pernot H, Costentin G (2012) ZnO oxygen vacancies formation and filling followed by in situ photoluminescence and in situ EPR. *J Phys Chem C* 116:21297–21307
- [63] Pan X, Yang MQ, Xu YJ (2014) Morphology control, defect engineering and photoactivity tuning of ZnO crystals by graphene oxide—a unique 2D macromolecular surfactant. *Phys Chem Chem Phys* 16:5589–5599